Genes, Brain and Behavior
Official publication of the International Behavioural and Neural Genetics Society

Genes, Brain and Behavior (2016) ***15:*** *491–502* doi: 10.1111/gbb.12292

CDKL5 knockout leads to altered inhibitory transmission in the cerebellum of adult mice

S. Sivilia[†], C. Mangano[†], S. Beggiato[‡], A. Giuliani[†], R. Torricella[§], V. A. Baldassarro[§], M. Fernandez[§], L. Lorenzini[§], L. Giardino[†,§], A. C. Borelli[‡], L. Ferraro[¶] and L. Calzà[†,§,,*]**

[†]Department of Veterinary Medical Science, University of Bologna, Bologna, [‡]Department of Medical Sciences, University of Ferrara, Ferrara, [§]Health Science and Technologies Interdepartmental Center for Industrial Research (HST-ICIR), University of Bologna, Bologna, [¶]Department of Life Sciences and Biotechnology, University of Ferrara, Ferrara, and [**]Department of Pharmacy and Biotechnology, University of Bologna, Bologna, Italy
**Corresponding author: L. Calzà, Health Science and Technology Interdepartmental Center for Industrial Research (HST-ICIR), University of Bologna, Via Tolara di Sopra 50, I-40064 Ozzano Emilia, Bologna, Italy. E-mail: laura.calza@unibo.it*

Mutations in the X-linked cyclin-dependent kinase-like 5 gene (*CDKL5*) are associated to severe neurodevelopmental alterations including motor symptoms. In order to elucidate the neurobiological substrate of motor symptoms in *CDKL5* syndrome, we investigated the motor function, GABA and glutamate pathways in the cerebellum of *CDKL5* knockout female mice. Behavioural data indicate that *CDKL5*-KO mice displayed impaired motor coordination on the Rotarod test, and altered steps, as measured by the gait analysis using the CatWalk test. A higher reduction in spontaneous GABA efflux, than that in glutamate, was observed in *CDKL5*-KO mouse cerebellar synaptosomes, leading to a significant increase of spontaneous glutamate/GABA efflux ratio in these animals. On the contrary, there were no differences between groups in K^+-evoked GABA and glutamate efflux. The anatomical analysis of cerebellar excitatory and inhibitory pathways showed a selective defect of the GABA-related marker GAD67 in the molecular layer in *CDKL5*-KO mice, while the glutamatergic marker VGLUT1 was unchanged in the same area. Fine cerebellar structural abnormalities such as a reduction of the inhibitory basket 'net' estimated volume and an increase of the pinceau estimated volume were also observed in *CDKL5*-KO mice. Finally, the *BDNF* mRNA expression level in the cerebellum, but not in the hippocampus, was reduced compared with WT animals. These data suggest that *CDKL5* deletion during development more markedly impairs the establishment of a correct GABAergic cerebellar network than that of glutamatergic one, leading to the behavioural symptoms associated with *CDKL5* mutation.

Keywords: CDKL5, cerebellum, GABA, gait, glutamate, pinceau

Received 8 October 2015, revised 13 January 2016, 2 March 2016 and 20 March 2016, accepted for publication 2 April 2016

Cyclin-dependent kinase-like 5 (*CDKL5*) is a gene located on the X chromosome also known as serine/threonine kinase 9 (STK9) (Montini *et al.* 1998). Since early description of chromosomal rearrangements involving this gene in two females (Kalscheuer *et al.* 2003), around 150 individuals (with a large prevalence of females) with a *CDKL5* mutation have been described and diagnosed with the early-onset seizure variant of Rett syndrome (RTT), autism, infantile spasms or West syndrome (Tao *et al.* 2004; Weaving *et al.* 2004). Thanks to the International RTT syndrome phenotype database (InterRett), it has been established that *CDKL5* disorder can be considered as an autonomous clinical entity (Bebbington *et al.* 2008; Fehr *et al.* 2013). The clinical features commonly associated with a *CDKL5* mutation include early-onset seizures, severe intellectual disability and gross motor impairment, mainly characterised by the delay in the ability to sit, independent walking, functional hand use, motor dyspraxia leading in some cases to impaired ambulation and severe hypotonia (Bahi-Buisson *et al.* 2008; Stalpers *et al.* 2012).

Little is known about the function and the mechanism of action of the protein. The *CDKL5* protein is involved in neuronal differentiation, dendritic arborization and synaptogenesis, recognising a number of substrates and affecting several genes (Chen *et al.* 2010). The *CDKL5* expression is strongly induced in early postnatal stages, and in the adult brain, *CDKL5* is present in mature neurons in the cerebral cortex, hippocampus, cerebellum and brain stem (Rusconi *et al.* 2008). Loss-of-function studies using RNA interference showed that *CDKL5* is required for neurite growth and excitatory synapse stability through Rac signalling remodelling of the actin fibres of cytoskeleton (Chen *et al.* 2010; Ricciardi *et al.* 2012). Mutations of *CDKL5* resulted in the loss of kinase activity towards its substrates (Sekiguchi *et al.* 2013), which includes the 120-kDa protein *amphiphysin 1*, a protein involved in clathrin-mediated endocytosis; *DNA methyltransferase 1* (Kameshita *et al.* 2008), and *netrin-G1 ligand*, a lipid-anchored protein that is structurally related to the netrin family of axon guidance molecules (Ricciardi *et al.* 2012). The *CDKL5* also mediates the phosphorylation of methyl-CpG-binding protein 2 (Mari *et al.* 2005), the protein encoded by *MECP2* gene which is considered to be the primary cause of RTT (Amir *et al.* 1999).

Two animal models lacking the *CDKL5* gene have been generated up-to-now. The mouse generated by Wang *et al.*

(2012) models a splice site mutation found in a *CDKL5* patient by deleting the mouse *CDKL5* exon 6 through homologous-mediated recombination in embryonic stem cells, thereby disrupting kinase activity. The mouse generated by Amendola *et al.* (2014) carries a constitutive knockout (KO) allele obtained by deletion of exon 4. The phenotypic characterisation of these mice shows autistic-like deficits in social interaction, impairments in fear memory, alterations in event-related potentials, disruption of multiple signal transduction pathways (Wang *et al.* 2012). Furthermore, limb clasping, hypoactivity, abnormal eye tracking, abnormal electroencephalograph responses to convulsant treatment, decreased visual evoked responses have been reported (Amendola *et al.* 2014). An impairment of hippocampus-dependent memory has been also described in this mouse (Fuchs *et al.* 2014). However, the neurobiological substrate of the complex behavioural phenotype produced by *CDKL5* mutation in human and mice is still unclear. In the attempt to overcome this gap, in this study, we investigated the neurochemical organisation of the cerebellum of *CDKL5* KO female mice (Amendola *et al.* 2014), with particular attention to the balance between the excitatory glutamate and inhibitory gamma-Aminobutyric acid GABA signalling. The cerebellum has been chosen in view of its role in movement planning and execution, and cognitive functions (Buckner 2013). Furthermore, in both mice and human, *CDKL5* is expressed in virtually all neurons, but not in astrocytes of the cerebellar granular (gl) and molecular (ml) layers and Purkinje (Pj) cells (Rusconi *et al.* 2008).

Materials and methods

Animals and genotyping

Mice were produced by crossing *CDKL5* heterozygos +/– female mice with *CDKL5* Y/– male, and *CDKL5* heterozygos +/– KO female mice with WT wilde type male mice (Amendola *et al.* 2014, the genetic background is C57BL/6J). The animals had access to water and food *ad libitum* and lived in a room with a 12:12 h dark/light cycle. Adult homozygous female (–/–, $N = 17$) and WT female (+/+, $N = 12$) were used in this study, housed in groups of three to four animals per cage.

Mice tails were used for genotyping analysis. The mice genomic DNA was extracted using the GenElute™ Mammalian Genomic DNA MiniPrep Kit (Sigma-Aldrich, Milan, Italy) according to the instructions of the manufacturer, and eluted in 100 µl of elution solution. The DNA concentration was determined using a spectrophotometer (Nanodrop 2000; Thermo Scientific, Waltham, MA, USA). The presence of the DNA deletion was identified by standard polymerase chain reaction (PCR) technique, using the enzyme GO TAQ Flexi DNA Polymerase (Promega, Milano, Italy) and specific primers. The sequences of the primers used for mice genotyping were the followings: 108F, F: 5′-ACGATAGAAATAGAGGATCAACCC-3′; 109R, F: 5′-CCCAAGTATACCCCTTTCCA-3′; 125R, F: 5′-CTGTGACTAGGGGCTAGAGA-3′.

For each sample the reaction was performed in a mix containing buffer 1×, $MgCl_2$ 1.5 mM, dNTPs 0.2 mM, primer 108F 1 µM, primer 109R 0.5 µM, primer 125R 0.5 µM, 1.25 U/µl of Taq polymerase and 100 ng/ml of DNA. After 4 min at 95°C, 33 PCR cycles were performed (94°C for 40 seconds, 59°C for 30 seconds, 72°C for 40 seconds), followed by 7 min at 72°C. Resulting PCR products were resolved by electrophoresis in a 2.0% agarose gel stained with Gel Red™ (Biotium, Hayward, CA, USA), using a 100 bp DNA ladder (Fermenta, Milano, Italy) as DNA marker. The 249 bp band represents the WT chromosome while the presence of a 344 bp band is because of the deletion. Results were obtained crossing the mice gender with the resulting PCR bands, as follows: WT male = 240 bp; CDKL5 Y/– male = 344 bp; WT female = 240 bp; CDKL5 heterozygos female = 344, 240 bp; CDKL5 homozygus female = 344 bp.

All the animal protocols described here were carried out in compliance with the European Community Council Directives of 24 November 1986 (86/609/EEC) and approved by our intramural committee and Ministero Salute, in accordance with the guidelines published in the Guide for the Care and Use of Laboratory Animals and ARRIVE guidelines.

Locomotion behavioural analysis

Cerebellar function was analysed by Rotarod and computerised gait analysis (Stroobants *et al.* 2013). Twelve animals were included in each group. Gait analysis was performed 7 days after Rotarod test. Tests were carried out in the light phase. To minimise stress, animals were individually handled daily for 10 min for 1 week before the behavioural experiments.

Motor coordination ability was tested using the LE 8500 RotaRod (2Biological Instruments, Varese, Italy), which consists of a central drum (6 cm diameter), gnarled to provide a suitable grip, elevated 20 cm above the floor. Mice were placed gently on the drum for three consecutive training days, performing four trials each day, accelerating from 4 to 40 r.p.m. for a maximum of 5 min with 1 h inter-trial interval. The latency to fall during the observation period was recorded (seconds) by the SEDACOM32 program version 1.0 (PanLab, Barcelona, Spain).

The CatWalk apparatus version 10.5 (Noldus Information Technology, Wageningen, the Netherlands), comprising a long glass plate with a fluorescent light beamed into the glass walkway floor, was used for computerised gait analysis, that was performed at least 1 week after the last Rotarod test (in 5.5-month-old animals). In a dim environment, the light is reflected downward and the footprints of the animal as it walks along the walkway are recorded by a camera mounted under the glass. Mice were trained to cross the walkway daily 1 week prior to the test. The mice performed uninterrupted runs for at least three times and the paw print footages were analysed by using the automated gait analysis system CatWalk software, classified and analysed using the Catwalk XT module (Bozkurt *et al.* 2008). The following parameters were considered: 'print area' (the total floor area contacted by the paw during the stance phase) and 'base of support (cm)' (the distance between the two hindpaw or forepaw measured perpendicularly to the direction of walking) as spatial static parameters of each paw; 'run duration' (the duration of the run based on the selected steps in the data selection), 'stand' (the duration in seconds of contact of a paw with the glass plate), 'swing' (the duration in seconds of no contact of a paw with the glass plate), 'swing speed' [the speed (distance unit/second) of the paw during swing] as kinetic parameters of each paw; 'stride length' [the distance (in distance units) between successive placements of the same paw], 'step cycle' (the time in seconds between two consecutive initial contacts of the same paw) as stride parameters; 'regularity index' (the number of normal step sequence patterns relative to the total number of paw placements) and 'cadence' (the number of steps) as gait coordination.

Spontaneous and K^+-evoked endogenous GABA and glutamate efflux from cerebellum synaptosome preparation

Crude synaptosome (P2) fraction was prepared from the cerebellum of six animals from each groups under investigation. Briefly, on the day of the experiment, a lightly anesthetised animal was sacrificed by decapitation and the cerebellum was dissected out from the brain. The tissue was then homogenised in ice-cold buffered (pH 7.4) sucrose solution (0.32 M). After the homogenate centrifugation (10 min; 2500 *g*, 4°C), the supernatant was collected and the synaptosomes were isolated by centrifugation (20 min; 9500 *g*, 4°C). The P2 pellet fraction was resuspended in 5 ml of Krebs solution (mM: NaCl 118.5, KCl 4.7, $CaCl_2$ 1.2, KH_2PO4 1.2, $MgSO_4$ 1.2, $NaHCO_3$ 25, glucose 10; gassed with 95% O_2/5% CO_2) (Chiodi *et al.* 2012).

After their preparation, the synaptosomes were maintained in warm condition (37°C) for 20 min. Thereafter, identical aliquots

(0.5 ml) of synaptosomal suspension were distributed on microporous filters, placed at the bottom of a set of parallel superfusion chambers, maintained at 37°C and continuously perfused with aerated (95% O_2/5% CO_2) Krebs solution (0.3 ml/min). After a 30-min wash-out period, nine consecutive 5-min fractions were collected. In details, after the collection of three basal samples, synaptosomes were depolarized with 15 mM K^+ for 90 seconds.

In each sample, GABA and glutamate levels were simultaneously measured by HPLC coupled with fluorimetric detection. Thirty microlitres per sample were transferred into glass microvials and placed in a temperature-controlled (4°C) Triathlon autosampler (Spark Holland, Emmen, The Netherlands). Before the injection, the system added 30 μl of *o*-phthaldialdehyde/mercaptoethanol reagent to each sample and, after 60 seconds of reaction, 40 μl of the mixture was injected onto a Chromsep analytical column (3 mm inner diameter, 10 cm length; Chrompack, Middelburg, The Netherlands). The column was eluted at a flow rate of 0.52 ml/min (Beckman 125 pump; Beckman Instruments Indianapolis, IN, USA) with a mobile phase containing 0.1 M sodium acetate, 10% methanol and 2.2% tetrahydrofuran (pH 6.5). Glutamate and GABA were detected by means of a Jasco fluorescence spectrophotometer FP-2020 Plus (Jasco, Tokyo, Japan). The retention times of glutamate and GABA were ~3.5 and ~15.0 min, respectively.

The GABA and glutamate efflux were expressed as pmol/min/g of protein while K^+-evoked GABA and glutamate efflux were expressed as percent increase over the respective spontaneous efflux (calculated by the mean of the two fractions collected prior to the depolarising stimulus). Protein was determined according to Bradford (1976).

Immunohistochemistry, microscopy, confocal microscopy and image analysis

Animals (six animals per group) were deeply anesthetised and perfused through the ascending aorta with physiological saline at 37°C (20 ml), followed by paraformaldehyde 4% (w/v) and 14% picric acid saturated aqueous solution in Sörensen buffer 0.1 M pH 7 at 37°C (20 ml) and at ice-cold temperature (20 ml). The brains were then removed and immersed for 90 min in the same ice-cold fixative, before being rinsed for at least 48 h in 5% sucrose in 0.1 M phosphate buffer. Cerebella were frozen in CO_2 and 14 μm thick cryostat sagittal sections (HM550 Microm, Bio-Optica, Milano, Italy) were collected on gelatin-coated slides from 1.95 mm to 1.525 lateral level according to Paxinos and Franklin (2001).

Sections were firstly incubated in 0.1 M phosphate buffered saline (PBS) at room temperature for 10–30 min, followed by overnight incubation at 4°C in a humid atmosphere with the primary antibodies diluted in 0.3% PBS–Triton X-100, v/v. The following antisera were used: goat, anti-calbindinD-28K (Santa Cruz Biotechnology, Dallas, TX, USA), 1:75; rabbit anti-vesicular glutamate transporter 1 (VGLUT1) (Abcam Cambridge, UK), 1:1000; mouse anti-glutamic acid decarboxylase 67 (GAD-67), Chemicon (Merck-Millipore, Darmstadt, Germany), 1:800; rabbit anti-post synaptic density protein 95 (PSD-95) (Abcam), 1:1000; mouse anti-neurofilament 200 (NF-200) (Sigma-Aldrich), 1:1000. After rinsing in PBS for 20 min (2 × 10 min), the sections were incubated at 37°C for 30 min in a humid atmosphere with the secondary antisera conjugated with different fluorochromes: DyLight488-conjugated affinity-pure Goat anti-Mouse IgG (Thermo Scientific, Monza, Italy), DyLight488-conjugated affinity-pure donkey anti-goat IgG (Jackson Immunoresearch, Suffolk, UK), Rhodamine Red™-X-conjugated-conjugated affinity-pure donkey anti-goat IgG (Jackson Immunoresearch) and Rhodamine Red™-X-conjugated affinity-pure donkey anti-rabbit IgG (Jackson Immunoresearch) diluted in 0.3% PBS–Triton X-100. Sections were then rinsed in PBS (as above) and mounted in glycerol containing 1,4-phenylendiamine (0.1 g/l).

In order to minimise technical bias, the following technical features were taken: all sections to be compared were processed in the same experimental session; five brains from different experimental groups were included in each slide, according to a random distribution; the same batch, dilution and preparation of primary such as secondary antibodies were used for all slides to be compared; the same conditions were established for all sections. For all indicated markers, three sections/animal were analysed, and the mean value/animal was used for the statistical analysis. All analyses were performed in blinded manner.

Immunofluorescence images were captured by a Nikon Eclipse E600 microscope (Nikon, Shinjuku, Japan) equipped with digital CCD (charged coupled device) camera Q Imaging Retiga-2000RV (Q Imaging, Surrey, BC, Canada). Measurements were performed using the NIS-Elements AR 3.2 software. The immunoreactive area was calculated as % area of the region of interest (ROI). The mean intensity was expressed as optical density (OD) of the immunoreactive signal, subtracted of the background.

For fine morphological analysis, sections were scanned with Nikon Ti-E fluorescence microscope coupled with A1R confocal system. Diode laser system with 405 wavelength output, air-cooled argon-ion laser system with 488 wavelength output, yellow diode-pumped solid-state laser system with 561 wavelength output and diode laser system with 638 wavelength output were used. Images were acquired with oil immersion × 60 with an optical resolution of 0.18 μm, using NIS-Elements AR 3.2 software (Nikon). All the *z*-stacks were collected in compliance with optical section separation (*z*-interval) values suggested by NIS-Elements AR 3.2 software. All the images to be compared were acquired using the same microscope configuration.

For the analysis of GAD-67 and VGLUT1 synaptic contacts, images were acquired with × 4 scanner zoom and 1024 × 1024 pixels resolution as confocal stacks with optical section separation (*z*-interval) of 0.4 μm and a *z*-volume of 6 μm. For the analysis of NF-200 around Pj cell body, images were acquired with 512 × 512 pixels resolution as confocal stacks with optical section separation (*z*-interval) of 0.2 μm and a *z*-volume of 8 μm. For the analysis of PSD-95, images were acquired with 1024 × 1024 pixels resolution as confocal stacks with optical section separation (*z*-interval) of 0.3 μm and a *z*-volume of 8 μm.

The number of synaptic spots was measured by three-dimensional (3D) voxel-based reconstruction followed by spot detection and count by Imaris BitPlane software 7.7.2 version (Bitplane AB, Saint Paul, MN, USA). The NF200- and PSD95-IR was detected by 3D voxel-based reconstruction on calibrated images, followed by filament and surface recognition, respectively, by Imaris BitPlane software, and finally referred as 'estimated volume'. 3D rendering of surfaces, spots and filaments are based on the identification of voxels belonging to an object (detected by their grey values). To create detailed surfaces and spots detection, we used confocal *z* stacks as source for Imaris 3D reconstruction and analysis. See *Results* for further details.

Total RNA isolation, reverse transcription and mRNA quantification

The cerebellum (six animals per group) was homogenised and total RNA isolation was performed using RNAeasy Mini Kit© (Qiagen, Milano, Italy). Total RNA was eluted in RNase-free water and using a spectrophotometer (Nanodrop 2000, Thermo Scientific), absorbance values at 260, 280 and 320 were measured.

The RNAs were subjected to DNase treatment (1 U/μl, 1× DNase buffer, 2 U/μl ribonuclease inhibitor, at 37°C for 30 min) (Fermentas) and were retrotranscribed using the enzyme M-Moloney murine leukaemia virus reverse transcriptase (M-MuLV-RT, 10 U/μl) (Fermentas), in the presence of 1× first strand buffer, 1 mM d(NTP)s (Fermentas), 25 ng/μl Oligo $(dT)_{18}$ primers (Fermentas) by incubating at 42°C for 60 min. A sample with no reverse transcriptase enzyme in the reaction mix was processed as NO-RT control.

Semi-quantitative real-time PCR was performed using the Mx3005P™ real-time PCR system (Stratagene, Santa Clara, CA, USA). The chemistry chosen to perform these PCR experiments was based on SYBR Green I fluorescent detection. Each reaction mix consisted of 10 ng of template cDNA, 1× Maxima™ SYBR Green/ROX qPCR Master Mix (Fermentas) and 0.4 μM of both primers (sense and antisense). Specific primers for each gene of interest were the followings: *GAPDH*, F: 5′-AAA GCC TCG TGC TGT CGG ACC-3′, R: 5′-GCA GGG TGG GTG TGC CGT C-3′; *BDNF*, F: 5′-GTG ACA GTA TTA GCG-3′, R: 5′-GCC TTC CTT CGT GTA ACC-3′; *VEGF*, F: 5′-AAG AGA AGG AAG AGG AGA G -3′, R: 5′-ACC CAA GAG AGC AGA AAG-3; *IGF1*, F: 5′-TCA TGT CGT CTT CAC ACC TCT T-3′, R: 5′-ACA CAC GAA CTG AAG AGC AT-3′; among these, *GAPDH* was

considered as housekeeping gene. All primers were obtained from IDT (Coralville, IA, USA).

In order to check for possible contamination of genomic DNA, the NO-RT control was processed. No template controls were also used for each reaction mix. Thermal profile of PCR reactions was performed as follow: an activation step of master mix Taq polymerase (95°C, 10 min) and 40 cycles of denaturation (95°C, 15 seconds) and annealing/extension (60°C for 30 seconds). At the end of the amplification cycles, the dissociation curve was obtained by following a procedure consisting of first incubating samples at 95 °C for 1 min to denature the PCR-amplified products, then ramping temperature down to 55°C and finally increasing temperature from 55 to 95°C at the rate of 0.2 C/second, continuously collecting fluorescence intensity over the temperature ramp.

The specificity of the amplified product was verified by the presence of a single peak at the expected melting temperature. Random amplified products were resolved by electrophoresis in a 2.0% agarose gel stained with Gel Red™ (Biotium) in order to check the specificity of the PCR reaction. This was confirmed by the presence of a single band of the expected size. A 100 bp DNA ladder (Fermentas) was used as DNA marker.

No significant variations were found in the expression of *GAPDH*, confirming its suitability as housekeeping gene. The semi-quantitative analysis of gene expression was performed on the values of the threshold cycle (Ct) obtained for each sample, considering *GAPDH* as housekeeping gene.

The efficiency of the primers used for real-time PCR reactions was calculated by amplifying control cDNA serial dilution. Standard curve slope and primer efficiency were calculated with the MxPro QPCR software 3.1 (Stratagene, La Jolla, CA, USA). Samples were always processed in duplicate. The relative gene expression was calculated by the formula $2^{(-\Delta\Delta Ct)}$ using a defined group as reference ($2^{(-\Delta\Delta Ct)} = 1$).

Western blot

For this experiment, four animals were included in each group. The cerebellum was homogenised twice using the Ultra Turrax homogenizer (IKA, Staufen, Germany) in ice-cold RIPA Radioimmunoprecipitation assay buffer lysis buffer: 150 mM NaCl, 50 mM Tris pH 8.0, 1% Triton X-100, 0.5% sodium deoxycholate and 0.1% sodium dodecyl sulphate supplemented with 1 mM phenylmethanesulphonylfluoride, 10 mM sodium fluoride, 1 mM sodium orthovanadate and 1% inhibitors cocktail (Sigma-Aldrich). Samples were then incubated in ice for 30 minutes and centrifuged at 13000 g for 20 minutes at 4°C.

Proteins in the supernatant fraction were quantified using the Lowry method. Equivalent amounts of protein (15 μg for cerebellum and hippocampus, 25 μg for cortex) were subjected to electrophoresis on 4–20% polyacrylamide Mini-protean TGXTMgels (Bio-Rad, Milano, Italy). The gel was then blotted onto a nitrocellulose membrane (Protran BA85 Whatman, Sigma-Aldrich), and equal loading of protein in each lane was assessed by brief staining of the blot with 0.1% Ponceau S (Sigma-Aldrich). Membranes were blocked for 1 h in 2.5% BSA (bovine serum albumine)/0.1% Tween-20 in PBS and incubated overnight in PBS/0.1% Tween-20 at 4°C with primary antibodies: anti-goat polyclonal, rabbit monoclonal anti-PSD-95 (Millipore, Darmstadt, Germany; dilution 1:1000), and rabbit polyclonal anti-β-Actin (Sigma-Aldrich; dilution 1:10 000). Membranes were washed, incubated with HRP-conjugated anti-rabbit, anti-goat or anti-mouse secondary antibodies (1:2000, Dako, Milano, Italy) and specific reactions revealed with the enhanced chemiluminescent (ECL) Clarity™ ECL Substrate (Bio-Rad). Densitometry analysis on digitised images was performed with Fluor-STM Multimager using the Quantity One software (Bio-Rad) version 4.2.1 (cerebellum) and Chemi DOCTM MP Imaging systems, using the softwae ImageLAB 5.2.1. (cerebral cortex and hippocampus). Intensity for each band was normalised to the intensity of the corresponding β-actin band. The relative protein content was expressed as arbitrary units.

Statistical analysis

Data from single animals were the unity of analysis in all experiments. Statistical testing was performed with two-way analysis of variance (ANOVA) followed by *post hoc* multiple comparisons test (accelerating Rotarod), and Student's *t*-test (overall Rotarod, and all other experiments). A probability level of $P < 0.05$ was considered to be statistically significant.

Data accessibility

The standard operating procedures used to plan the study and conduct all experiments, all raw data (including CatWalk movies) generating the complete data-set used for manuscript, figures preparation and statistical analysis are available upon editorial request.

Results

Animals and locomotion analysis

Breeding, nursing and weaning were comparable in all genotypes, and no spontaneous mortality was observed over the experimental time.

The motor performance in accelerating Rotarod test was evaluated in 2.5-month-old animal and re-tested in the same animal when 5.5 months old. Results are presented in Fig. 1, where graph A refers to the test performed in 2.5-month-old mice and graph B to the re-test in 5.5-month-old mice. The overall evaluation of performance (from trial 1 to 12) indicates that *CDKL5* mutated animals fell down earlier compared with the respective WT (two-way ANOVA, genotype effect: $F(1,26) = 7.933$, $P = 0.0091$). Moreover, a trial effect is also observed, showing an impairment in Rotarod learning in *CDKL5* mutated animals (two-way ANOVA, trial effect: $F(11\ 286) = 2.289$, $P = 0.0108$; genotype × trial interaction: $F(11\ 286) = 3.074$, $P = 0.0006$). We re-tested animal at the time of sacrifice (graph B), confirming that the motor coordination defect in –/– mice was still present (two-way ANOVA, genotype effect: $F(1,25) = 11.91$, $P = 0.0020$).

Results from gait and CatWalk computerised analysis are reported in Table 1 and analysed by Student's *t*-test. A significant alteration in the spatial single paw support is observed in *CDKL5* –/– mice, which was characterised by a decreased print area (fore paw: $P = 0.0016$; hind paw: $P = 0.0156$) and base of support ($P = 0.0074$). Moreover, the duration of contact of hind paws with the glass plate was shorter in *CDKL5* –/– mice than in WT +/+ mice ($P = 0.0314$).

GABA and glutamate efflux from cerebellar and hippocampal synaptosomes

Spontaneous and K^+-evoked endogenous GABA and glutamate efflux from synaptosomes obtained from *CDKL5* –/– compared with the WT mice have been evaluated. A nearly four- and twofolds reduction in spontaneous GABA and glutamate efflux, respectively, was observed in cerebellum synaptosomes from *CDKL5* –/– mice (Fig. 2a, $P = 0.0009$; Fig. 2b, $P = 0.0324$). There were no significant changes in spontaneous GABA and glutamate efflux in cerebellar synaptosomes (Fig. 2b). However, a trend to a reduction was observed in synaptosomes from *CDKL5* –/– mice. Based on the above results, the glutamate/GABA efflux ratio in cerebellar synaptosomes from each animal was calculated. Interestingly, a significant increase of this ratio was observed in *CDKL5* –/– mice when compared with WT animals (Fig. 2c).

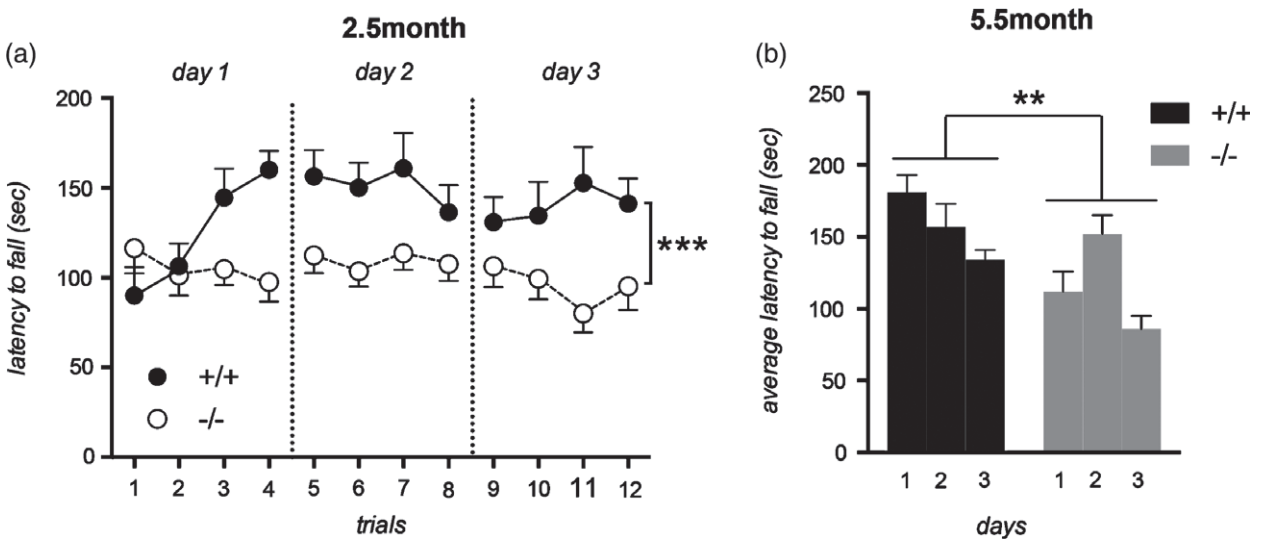

Figure 1: Somatosensory integration tested by accelerating Rotarod in CDKL5 −/− (*N* = 17) and WT (*N* = 12) female mice. Data are expressed as mean ± SEM (standard error of mean). In (a), each point represents the latency to fall down in the fourth session during the three consecutive days of the test. Graph (b) shows performance of the same animal at 5.5 months of age, analysed by pooling the trials of each day to limit motivation and motor learning bias. Values represent the average mean latency to fall expressed in seconds ± SEM. Statistical analysis: two-way ANOVA and *post hoc* Bonferroni's test, $^{**}P < 0.005$; $^{***}P < 0.001$.

Table 1: CatWalk analysis of individual paw and gait parameters

Parameter			WT	−/−
(a) Spatial paw	Print area	Fore	0.283 ± 0.012	0.209 ± 0.015**
		Hind	0.228 ± 0.014	0.171 ± 0.016*
	Base of support (cm)	Hind	1.545 ± 0.048	1.348 ± 0.048**
		Fore	2.688 ± 0.093	2.782 ± 0.124
(b) Kinetic paw	Run duration (second)		1.974 ± 0.176	1.873 ± 0.117
	Stand (second)	Fore	0.148 ± 0.009	0.130 ± 0.005
		Hind	0.143 ± 0.007	0.121 ± 0.007*
	Swing (second)	Fore	0.117 ± 0.005	0.119 ± 0.003
		Hind	0.109 ± 0.005	0.115 ± 0.005
	Swing speed (cm/second)	Fore	65.24 + 3.820	63.70 ± 2.04
		Hind	64.31 + 4.087	61.09 ± 2.36
(c) Comparative paw	Stride length (cm)	Fore	6.892 ± 0.222	7.270 ± 0.118
		Hind	6.514 ± 0.262	6.879 ± 0.156
	Step cycle (second)	Fore	0.269 ± 0.013	0.248 ± 0.006
		Hind	0.257 ± 0.011	0.235 ± 0.006
(d) Coordination	Regularity index (%)		94.21 ± 2.021	93.80 ± 1.512
	Cadence		16.49 ± 1.026	16.48 ± 0.629

Twelve animals were included in each group. Statistical analysis: Student's *t*-test, $^{*}P < 0.05$; $^{**}P < 0.01$.

As shown in Fig. 2d,e, there were no differences between groups in K^+-evoked endogenous GABA and glutamate efflux from cerebellar synaptosomes, calculated as percent increase over the respective spontaneous efflux. By comparing spontaneous and K^+-evoked endogenous GABA and glutamate efflux from hippocampal synaptosomes obtained from *CDKL5* −/− with those measured in WT mice, only a significant reduction in spontaneous GABA efflux was observed. However, the reduction in spontaneous GABA efflux obtained in hippocampal synaptosomes from *CDKL5* −/− mice was lower than that observed in the cerebellum (*CDKL5* −/− = 22.67 ± 5.38 pmol/min/g of protein; WT +/+ = 45.27 ± 6.15 pmol/min/g of protein; $P < 0.05$) (data not shown).

GABAergic and glutamatergic pathways in the cerebellum

In view of the above results, possible alterations of cerebellar excitatory and inhibitory pathways have been evaluated in CDKL5 −/− mice. Glutamic acid decarboxylase (GAD67) and

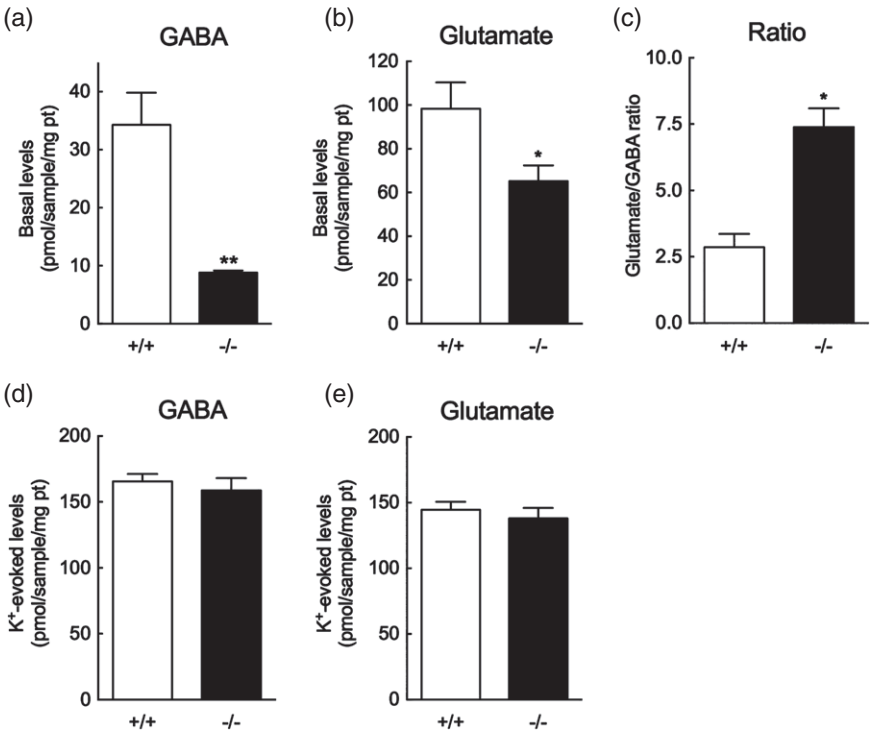

Figure 2: The GABA and glutamate efflux from cerebellar synaptosomes. (a, b, d, e) Basal and K^+-evoked GABA (a, d) and glutamate (b, e) efflux from synaptosomes isolated from the cerebellum. The GABA and glutamate efflux is expressed as pmol/min/g of protein while K^+-evoked GABA and glutamate efflux is expressed as percent increase over the respective spontaneous efflux (calculated by the mean of the two fractions collected prior to the depolarising stimulus). Eight-nine animals were included in each group. Data are expressed as mean ± SEM. Statistical analysis: Student's *t*-test, $*P < 0.05$; $**P < 0.001$. (c) Basal glutamate/GABA efflux ratio in synaptosomes isolated from the cerebellum. Data are expressed as mean ± SEM. Statistical analysis: Student's *t*-test, $*P < 0.05$.

VGLUT1 were used as markers for inhibitory and excitatory synaptic contacts, respectively (Kaneko *et al.* 2002).

Figure 3 shows the representative images of GAD67-IR (a, b) and VGLUT-IR (c, d) in the cerebellar cortex of WT and *CDKL5* –/– female mice. The analysis of immunoreactivity (IR) has been carried out in the gl and ml layer. We evaluated both IR [immunoreactive area (IR % area) or immunoreactive mean intensity (OD)] and the number of 'puncta' in the layers of interest, thus estimating both the size/number of the structural elements (IR % area) and the expression level/staining intensity (proportional to the antigen content) in each element (OD). The number of synaptic contacts was calculated using the Imaris 'spot' program, which allows to semi-automatically identify point-like ('puncta') structures in 3D images (Fig. 3e–g). We first estimated the mean spot diameter (around 0.3 μm) using the 'slice visualisation tool' in both WT and *CDKL5* –/– mice. Positive spots in the area of interest were then automatically selected by applying the 'quality filter', which classifies the spots based on the intensity at the centre.

Results of quantifications are reported in Fig. 3h–j (GAD67-IR) and Fig. 3k–m (VGLUT-IR). A general decrease of GAD67-IR in the ml (IR % area: $P = 0.0217$; no. of spots: $P < 0.0001$) and gl ($P = 0.0017$) layers was observed in *CDKL5* –/– mice when compared with WT +/+ mice. No differences between the genotypes were observed by evaluating the VGLUT-IR.

The fibre net around the Pj cell soma visualised by neurofilament-heavy chain (NF-200) reflecting the inhibitory synaptic inputs from the basket cells, was then evaluated. Figure 4a shows a confocal image of NF200-IR net (red) around the calbindin-positive soma (green) of Pj cells. The net was calculated cell-by-cell, selecting a ROI for each cell body by means of Imaris 'filament' program on confocal images (Fig. 4b,c). Being threshold based, the filament program uses the AutoPath tracking function to trace filaments. This algorithm is based on local intensity contrast and connects large start- and small end-points, producing a tree-like filament. We first defined the ROI, the source channel along with the thinnest (filament ending) and the largest diameter (filament beginning). Using the absolute intensity histogram, we then selected starting and seed points along with the threshold, on the basis of the 'shortest distance from distance map' algorithm, to calculate the filament estimated volume. As shown in Fig. 4d, the estimated volume of the NF200-IR GABA-ergic basket cell innervation was lower in *CDKL5* –/– mice than in WT +/+ animals ($P = 0.0212$).

Finally, the ramified axons of basket cells forming the 'pinceau' (Cajal 1911) that embraces the initial segment of cerebellar Pj cell axons have been evaluated. This structure was visualised by PSD-95-IR (Iwakura *et al.* 2012) (Fig. 4e–g). The PSD-95 IR estimated volume and the staining intensity of GAD-67-IR in the pinceau (Fig. 4i–k) were measured. The pinceau estimated volume was calculated cell-by-cell, building a surface for each cell, and using the absolute intensity histogram to select the PSD95-positive voxels, only, and excluding the background. The pinceau estimated volume was higher in *CDKL5* –/– than in WT +/+ mice (Fig. 4h; $P = 0.0492$), while the GAD-67-IR intensity as measured in the 3D-rendering used to calculate the pinceau estimated volume, was similar in the two genotypes (Fig. 4l).

In order to establish whether the enlargement of the pinceau corresponded to an increase in PSD-95 protein, PSD-95 content was also assessed by Western blot. The

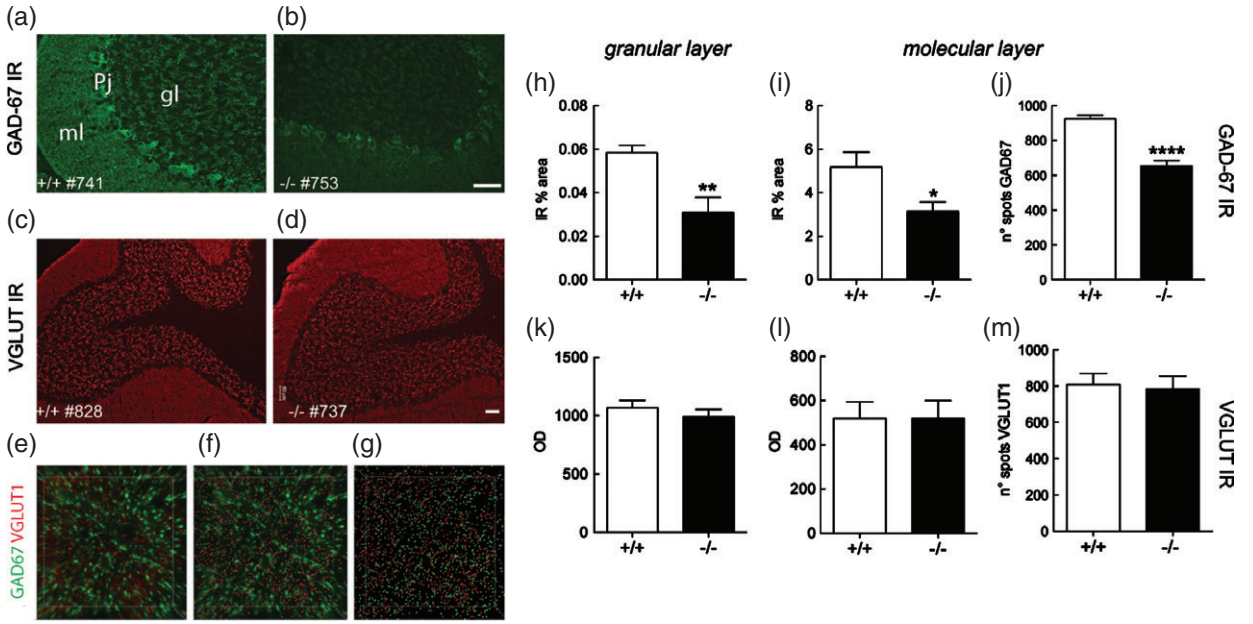

Figure 3: Analysis of GABA-ergic and glutamatergic markers in the cerebellar cortex of CDKL5 −/− and WT animals. (a, b): representative images of GAD-67-IR in WT (a) and *CDKL5* −/− (b) mice. (c, d) Representative images of VGLUT1-IR in WT (c) and *CDKL5* −/− (d) mice; (e–g) step by step scheme of 3D analysis of VGLUT1 (red channel) and GAD67 (green channel) positive spots in the ml layer of cerebellum; each channel is built separately and the number of VGLUT1 and GAD67-positive spots was calculated. (h–j) Semi-quantitative analysis of GAD67-IR in the gl (H) and ml layers (i, j), expressed as immunoreactive % area (h, i) and number of positive puncta in a standard area (j, area 26.5 μm^2). (k–m) Semi-quantitative analysis of VGLUT1-IR in the gl (k) and ml layers (l, m), expressed as OD (k, l) and number of positive puncta in a standard area (m, area 26.5 μm^2). The numbers in (a–d) refer to the animal code. Six animals were included in each group. Data area expressed as mean ± SEM. Statistical analysis: Student's *t*-test, *P < 0.05; **P < 0.01; ***P < 0.001; ****P < 0.0001. Scale bars: 50 μm. gl, granular layer; ml, molecular layer; Pj, Purkinje cells.

protein level was higher in *CDKL5* −/− than in WT +/+ mice (Fig. 4m; $P = 0.0414$) in the cerebellum, but not in the cerebral cortex and in the hippocampus.

Neurotrophins and growth factors mRNA expression levels in the cerebellum

Because of the unbalance between excitatory and inhibitory neurotransmission in the cerebellum observed in *CDKL5* −/− compared with WT +/+ mice, and because the expression level of several neurotrophins is regulated by neural activity (Kuczewski *et al.* 2010), the expression levels of mRNA encoding for some neurotrophic and growth factors were assessed. The *BDNF* (brain derived neurotrophic factor) mRNA expression level was strongly reduced in the cerebellum ($P = 0.0129$), but not in the hippocampus, of *CDKL5* −/− compared with WT mice (Fig. 5). No differences between the two genotypes in the mRNA expression levels of the *BDNF* high-affinity receptor *trkB*, (tropomyosine receptor kinase B) *VEGF* and (vascular endothelial growth factor) *IGF1* were (insulin-like growth factor 1) observed (data not shown).

Discussion

The impact of the deletion of CDKL5 protein on neurodevelopment has been mainly investigated in the hippocampus and cerebral cortex of *CDKL5*-KO mice. An alteration of postnatal neurogenesis and hippocampal-dependent behaviours (Fuchs *et al.* 2014), a reduced dendritic arborization of cortical neurons (Amendola *et al.* 2014), and altered auditory-evoked event-related potential (Wang *et al.* 2012) have been described. In this study, we indicate that cerebellum is also affected by *CDKL5* deletion. In particular, our results indicate severe alteration in the excitatory and inhibitory transmitters in the cerebellum of *CDKL5* KO compared with WT, and this is associated to an altered locomotor behaviour involving sensory-motor integration and gait.

CDKL5 mutated animals have a severe motor imbalance

The *CDKL5* mutations in humans are associated with severe motor symptoms, including gait dysfunction, spasticity and movement disorders (Bahi-Buisson *et al.* 2008; Stalpers *et al.* 2012). *CDKL5* KO mice show a significant hypolocomotion in home cage (Amendola *et al.* 2014), while an impairment in motor coordination has been described in the Wang's animal model (Wang *et al.* 2012). In this study, we demonstrate that the impairment in motor coordination is also present in the *CDKL5* KO mouse model generated by Amendola *et al.* (2014). In addition, we also performed, for the first time, the gait analysis of *CDKL5* mutated female mice. Thus, we demonstrate the presence of an alteration in gait in *CDKL5*

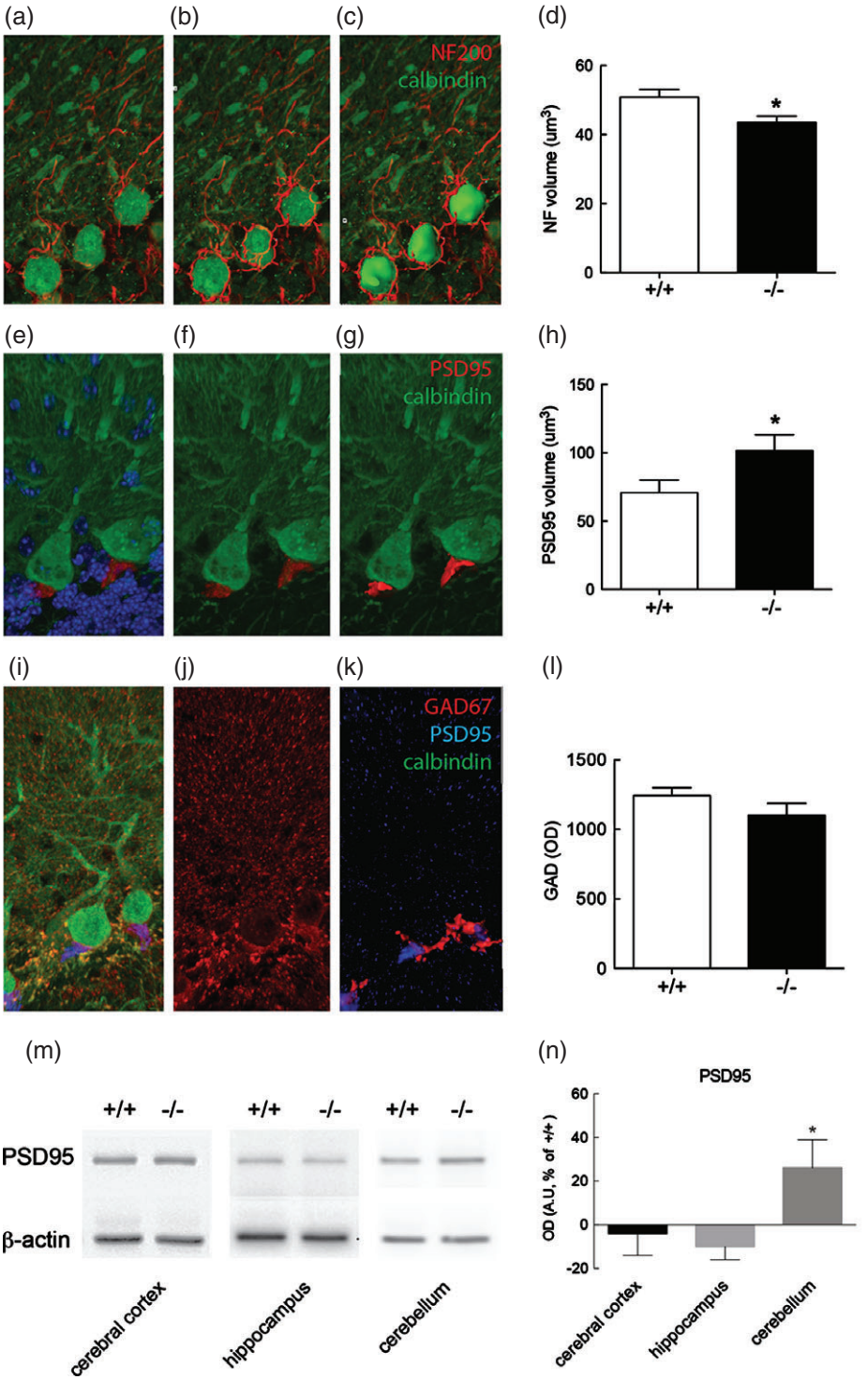

Figure 4: Fine neurochemical analysis of inhibitory inputs to the Pj cells in the cerebellar cortex of female *CDKL5* −/− and WT animals. (a–c) Step by step 3D analysis of the NF200-IR-positive 'net' (red channel) surrounding Pj cell body (as identified by calbindin D28K-IR, green channel) and net volume quantification (d). (e–g) Step by step 3D analysis of the PSD-95-IR 'pinceau' (red channel), surrounding the Pj cells hillock (as identified by calbindinD28K-IR, green channel). The surface was built in order to calculate the PSD95-IR volume (h). (i–k) GAD-67 [(j), red channel and (k) 3D identification], PSD95 [(i) and (k) blue channel] and merged image (i) in Pj cells, as identified by calbindinD28K-IR (green channel), and quantification of GAD-67 staining intensity (l). Six animals were included in each group. Results are expressed as mean ± SEM. Statistical analysis: Student's *t*-test, $*P < 0.05$. (m) Representative images of PSD95 Western blot in the cerebral cortex, hippocampus and cerebellum of *CDKL5* −/− and WT animals and quantification (n). Data are the % change in *CDKL5* −/− respect to WT animals and expressed as mean ± SEM. Statistical analysis: Student's *t*-test, $*P < 0.05$.

−/− mice, characterised by a decreased print area, possibly because of a 'tiptoed' locomotion or a 'closed finger walking', correlated to a decreased 'stand' duration. The 'base of support' is also decreased for the fore, but not hindpaw *CDKL5* −/− mice, suggesting that mutated animals need to have a wider base of support in posterior paws during locomotion than WT, possibly to compensate balance defects. Notably, a similar gait abnormality has been described in the mouse model for Refsum disease characterised by ataxia (Ferdinandusse *et al.* 2008).

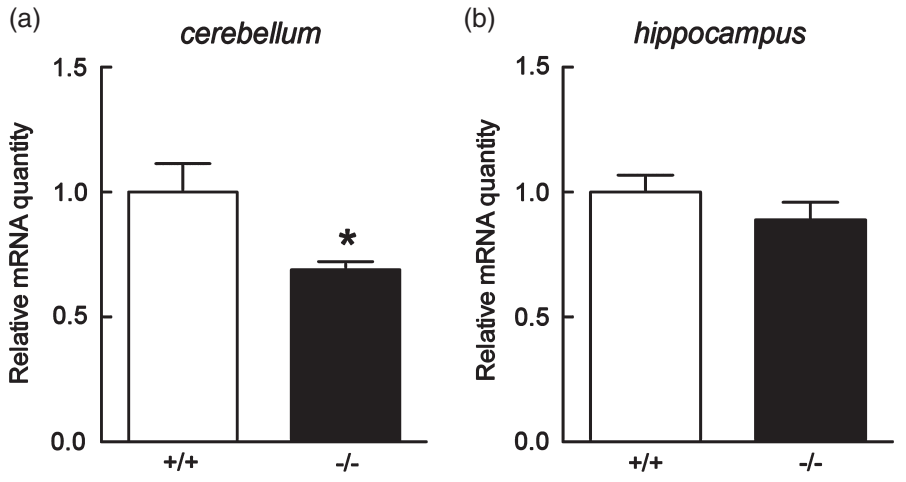

Figure 5: The *BDNF* mRNA expression levels in the cerebellum and hippocampus of female *CDKL5* −/− and WT animals. The graphs represent the relative mRNA expression of *BDNF* normalised vs. the WT animals. Six animals were included in each group. Data are expressed as mean ± SEM. Statistical analysis: Student's *t*-test, $*P < 0.05$.

The role of the cerebellum in achieving either movement skills in humans (Obayashi 2004; Timmann *et al.* 2001) and motor coordination in rodents (Kayakabe *et al.* 2014; Zhang *et al.* 2014), led us to hypothesise that alterations in cerebellar neurotransmission and/or neuroanatomy might underlie the motor coordination impairment observed in *CDKL5* KO mice.

However, we should also consider that the observed behavioural phenotype could be a consequence of a GABA or glutamate defect during development, being both aminoacids morphogens during development (Huang *et al.* 2007; Manent & Represa 2007; Takayama 2005).

CDKL5 deletion induces a GABA/glutamate unbalance in the cerebellum

Considering that GABA and glutamate are the main neurotransmitters in the cerebellum (Nakanishi 2005), we firstly evaluated spontaneous and K^+-evoked endogenous GABA and glutamate efflux from synaptosomes (e.g. isolated synaptic terminals) obtained from WT and *CDKL5* KO mice. A higher reduction in spontaneous GABA efflux, compared with that in spontaneous glutamate efflux, was observed in *CDKL5* −/− mouse-isolated nerve terminals. The present results suggest that GABA neurons are more markedly affected by the loss of *CDKL5* than the glutamate ones. In accordance, we found an unbalance between these inhibitory and excitatory transmitters in the cerebellum of *CDKL5* −/− mice, as demonstrated by the increase of glutamate/GABA ratio, in these mutated animals. Whether motor coordination impairment in mutated mice depends on this unbalance cannot be determined at this point. In this context, it is worth noting that the motor coordination impairment, observed in a transgenic animal model of progressive ataxia (Massella *et al.* 2009), was associated with a decrease in cerebellar GABA content. Thus, the reduced cerebellar GABA signalling in *CDKL5* −/− mice, and the consequent increase in glutamate/GABA ratio, might contribute, at least partially, to their motor coordination dysfunctions. Finally, the evidence that there were no differences between groups in K^+-evoked endogenous GABA and glutamate efflux suggests that *CDKL5* −/− mouse cerebellar GABA and glutamate nerve terminals maintain their stimulus-dependent exocytotic activity.

The altered neurotransmitter profile in *CDKL5* −/− mouse could also impact on cerebellum development. In particular, several lines of evidence indicates that a reduction of GABAergic signalling during development leads to a severe unbalance between excitatory and inhibitory transmitters in neuronal circuits during adulthood, possibly leading to behavioural deficit also in RTT phenotype (Hirano *et al.* 2002; Wulff *et al.* 2009; Chao *et al.* 2010).

CDKL5 deletion induces an alteration in excitatory/inhibitory circuits in the cerebellum

The possible mechanism linking *CDKL5* mutation to the described neurochemical unbalance in spontaneous glutamate and GABA efflux from cerebellar synaptosomes is not clear. *CDKL5* expression is highly regulated during development, being involved in neuronal maturation and maintenance, neuronal cytoskeleton rearrangement, dendrite growth and synaptic activity (Chen *et al.* 2010; Kilstrup-Nielsen *et al.* 2012; Della Sala & Pizzorusso 2014). In the cerebellum, *CDKL5* appears at P5 and reaches the peak in the adult brain, where it is localised in almost all neurons (Rusconi *et al.* 2008). Moreover, *CDKL5* is present in both glutamatergic and GABAergic primary cultured neurons, the expression levels being higher in the latter cell population (Rusconi *et al.* 2008). Thus, the lack of *CDKL5* during the development might affect the cerebellar connectivity development and related neurochemistry. These findings, together with the above-reported neurochemical results, prompted us to perform an anatomical analysis of cerebellar excitatory and inhibitory pathways in *CDKL5* −/− mice. In particular, we analysed synaptic contacts and organisation in the cerebellar cortex focusing on GABA and glutamate markers. Punctate positivity for *GAD-67* is related to putative GABAergic nerve terminals (Benagiano *et al.* 2000) arising from a number of inhibitory interneurons, including Golgi-, basket-, stellate-cells (Hashimoto & Hibi 2012). When analysed in the ml layer, VGLUT1-IR reflects parallel fibres (thus, axons from granule cells), while in the gl layer, it reflects mossy fibres

(thus, cerebellar afferences from pontine nuclei, etc.). The neuroanatomical analysis shows a defect of GAD-67 in the gl and ml layer of *CDKL5* –/– mice, where GABAergic basket and stellate interneurons are located. Notably, the glutamatergic marker VGLUT1 is unchanged in the same area, thus supporting the existence of an unbalance between glutamatergic and GABAergic inputs, as observed in neurochemical experiment. Notably, also *MeCP2* deletion in RTT appears to produce alterations of structural synaptic plasticity in inhibitory, but not excitatory, circuits in the cerebellum (Lonetti *et al.* 2010). Moreover, we found that the estimated volume of the basket 'net' carrying inhibitory synaptic inputs from the basket cells to the Pukinje cells, is decreased in *CDKL5* –/– mice compared with WT +/+ animals, reflecting a structural abnormality or a decreased antigen content. The same fibres extend to wrap around the initial segment of the Pj cell axon in a structure called the pinceau (Cajal 1911). This structure can be visualised by PSD-95 (Buttermore *et al.* 2012). In fact, although PSD-95 is mainly associated to the post-synaptic density of excitatory synapses through the brain (El-Husseini *et al.* 2000), in the adult cerebellum is localised to pre-synaptic terminals of GABA-ergic synapses, specifically to the specialised basket cell terminal pinceau (Castejón *et al.* 2004). This structure possibly mediates inhibition via the electrical field surrounding the Pj cell axon initial segment (Blot & Barbour 2014). Strikingly, we observed an increase in the pinceau estimated volume in *CDKL5* –/– mice compared with WT +/+ animals. Moreover, we also found an increase in the content of PSD-95 in the cerebellum, but not in the cerebral cortex and hippocampus, of *CDKL5* –/– mice compared with WT +/+ animals. Being PSD-95 in the adult cerebellum exclusively localised in the pinceau, this finding supports the existence of an alteration of this structure in *CDKL5* –/– mice. It is worth noting that the regular pinceau organisation is required for normal motor behaviours including gait (Bobik *et al.* 2004; Suárez *e*t al. 2008). Thus, it might be speculated that the alteration of this structure could participate to the behavioural impairments observed in *CDKL5* –/– adult mice.

CDKL5 deletion induces an impairment in BDNF mRNA expression in the cerebellum

The *BDNF* is highly expressed in the cerebellum through adulthood (Lindholm *et al.* 1994), where it plays a key role in regulating the structure and phenotype of mature neurons (Lindholm *et al.* 1997). In particular, the activity-dependent regulation of *BDNF* expression is a critical event in synaptic plasticity (Kohara *et al.* 2001), and an altered glutamate-receptor-mediated *BDNF* mRNA expression has been described in *stargazer* mice, characterised by ataxia, motor dyskinesia and epilepsy (Meng *et al.* 2007). In this study, we observed a reduction of *BDNF* mRNA expression level in the cerebellum of *CDKL5* –/– mice. Other growth factors (*NGF* (nerve growth factor), *IGF-1* and *VEGF*) are not modified, and *BDNF* itself is not altered in other brain areas, like hippocampus. While specific experiments are necessary to evaluate the developmental profile and the regulation of *BDNF* synthesis by excitatory stimuli, we can argue that the defect of basal synthesis of *BDNF* in adult *CDKL5* –/– mice might also be part of the complex neurochemical dysregulation observed in these animals.

Conclusions

Collectively, this study suggests that *CDKL5* deletion during development severely affects the establishment of a correct GABAergic network in the cerebellar cortex, as indicated by the 3.9-fold decrease of GABA efflux in respect to the 1.51 decrease of glutamate efflux, along with a general decrease in the inhibitory puncta density. The *CDKL5* deletion itself, or the GABA decline eventually derived from *CDKL5* deletion during development, could then lead to alterations in cerebellum neurochemistry and fine anatomy supporting the motor symptoms associated to *CDKL5* mutation.

References

Amendola, E., Zhan, Y., Mattucci, C., Castroflorio, E., Calcagno, E., Fuchs, C., Lonetti, G., Silingardi, D., Vyssotski, A.L., Farley, D., Ciani, E., Pizzorusso, T., Giustetto, M. & Gross, C.T. (2014) Mapping pathological phenotypes in a mouse model of CDKL5 disorder. *PLoS One* **9**, e91613.

Amir, R.E., Van den Veyver, I.B., Wan, M., Tran, C.Q., Francke, U. & Zoghbi, H.Y. (1999) Rett syndrome is caused by mutations in X-linked MECP2, encoding methyl-CpG-binding protein 2. *Nat Genet* **23**, 185–188.

Bahi-Buisson, N., Nectou, J., Rosas-Vargas, H., Milh, M., Boddaert, N., Girard, B., Cances, C., Ville, D., Afenjar, A., Rio, M., Héron, D., N'guyen Morel, M.A., Arzimanoglou, A., Philippe, C., Jonveaux, P., Chelly, J. & Bienvenu, T. (2008) Key clinical features to identify girls with CDKL5 mutations. *Brain* **131**, 2647–2661.

Bebbington, A., Anderson, A., Ravine, D., Fyfe, S., Pineda, M., de Klerk, N., Ben-Zeev, B., Yatawara, N., Percy, A., Kaufmann, W.E. & Leonard, H. (2008) Investigating genotype-phenotype relationships in Rett syndrome using an international data set. *Neurology* **70**, 868–875.

Benagiano, V., Virgintino, D., Rizzi, A., Flace, P., Troccoli, V., Bormann, J., Monaghan, P., Robertson, D., Roncali, L. & Ambrosi, G. (2000) Glutamic acid decarboxylase-positive neuronal cell bodies and terminals in the human cerebellar cortex. *Histochem J* **32**, 557–564.

Blot, A. & Barbour, B. (2014) Ultra-rapid axon-axon ephaptic inhibition of cerebellar Purkinje cells by the pinceau. *Nat Neurosci* **17**, 289–295.

Bobik, M., Ellisman, M.H., Rudy, B. & Martone, M.E. (2004) Potassium channel subunit Kv3.2 and the water channel aquaporin-4 are selectively localized to cerebellar pinceau. *Brain Res* **1026**, 168–178.

Bozkurt, A., Deumens, R., Scheffel, J., O'Dey, D.M., Weis, J., Joosten, E.A., Führmann, T., Brook, G.A. & Pallua, N. (2008) CatWalk gait analysis in assessment of functional recovery after sciatic nerve injury. *J Neurosci Methods* **173**, 91–98.

Bradford, MM (1976) A rapid and sensitive method for the quantitation of microgram quantities of protein utilizing the principle of protein-dye binding. *Anal. Biochem.* **72**, 248–254.

Buckner, R.L. (2013) The cerebellum and cognitive function: 25 years of insight from anatomy and neuroimaging. *Neuron* **80**, 807–815.

Buttermore, E.D., Piochon, C., Wallace, M.L., Philpot, B.D., Hansel, C. & Bhat, M.A. (2012) Pinceau organization in the cerebellum requires distinct functions of neurofascin in Purkinje and basket neurons during postnatal development. *J Neurosci* **32**, 4724–4742.

Cajal, S.R. (1911) *Histologie du système nerveux de l'hommes et des vertébrés*. Maloine, Paris.

Castejón, O.J., Fuller, L. & Dailey, M.E. (2004) Localization of synapsin-I and PSD-95 in developing postnatal rat cerebellar cortex. *Brain Res Dev Brain Res* **151**, 25–32.

Chao, H.T., Chen, H., Samaco, R.C., Xue, M., Chahrour, M., Yoo, J., Neul, J.L., Gong, S., Lu, H.C., Heintz, N., Ekker, M., Rubenstein, J.L., Noebels, J.L., Rosenmund, C. & Zoghbi, H.Y. (2010) Dysfunction in GABA signalling mediates autism-like stereotypies and Rett syndrome phenotypes. *Nature* **468**, 263–269.

Chen, Q., Zhu, Y.C., Yu, J., Miao, S., Zheng, J., Xu, L., Zhou, Y., Li, D., Zhang, C., Tao, J. & Xiong, Z.Q. (2010) CDKL5, a protein associated with Rett syndrome, regulates neuronal morphogenesis via Rac1 signaling. *J Neurosci* **30**, 12777–12786.

Chiodi, V, Uchigashima, M, Beggiato, S, Ferrante, A, Armida, M, Martire, A, Potenza, RL, Ferraro, L, Tanganelli, S, Watanabe, M, Domenici, MR, Popoli, P (2012) Unbalance of CB1 receptors expressed in GABAergic and glutamatergic neurons in a transgenic mouse model of Huntington's disease. *Neurobiol. Dis.* **45**, 983–991.

Della Sala, G. & Pizzorusso, T. (2014) Synaptic plasticity and signaling in Rett syndrome. *Dev Neurobiol* **74**, 178–196.

El-Husseini, A.E., Schnell, E., Chetkovich, D.M., Nicoll, R.A. & Bredt, D.S. (2000) PSD-95 involvement in maturation of excitatory synapses. *Science* **290**, 1364–1368.

Fehr, S., Wilson, M., Downs, J., Williams, S., Murgia, A., Sartori, S., Vecchi, M., Ho, G., Polli, R., Psoni, S., Bao, X., de Klerk, N., Leonard, H. & Christodoulou, J. (2013) The CDKL5 disorder is an independent clinical entity associated with early-onset encephalopathy. *Eur J Hum Genet* **21**, 266–273.

Ferdinandusse, S., Zomer, A.W., Komen, J.C., van den Brink, C.E., Thanos, M., Hamers, F.P., Wanders, R.J., van der Saag, P.T., Poll-The, B.T. & Brites, P. (2008) Ataxia with loss of Purkinje cells in a mouse model for Refsum disease. *Proc Natl Acad Sci U S A* **105**, 17712–17717.

Fuchs, C., Trazzi, S., Torricella, R., Viggiano, R., De Franceschi, M., Amendola, E., Gross, C., Calzà, L., Bartesaghi, R. & Ciani, E. (2014) Loss of CDKL5 impairs survival and dendritic growth of newborn neurons by altering AKT/GSK-3β signaling. *Neurobiol Dis* **70**, 53–68.

Hashimoto, M. & Hibi, M. (2012) Development and evolution of cerebellar neural circuits. *Dev Growth Differ* **54**, 373–389.

Hirano, T., Watanabe, D., Kawaguchi, S.Y., Pastan, I. & Nakanishi, S. (2002) Roles of inhibitory interneurons in the cerebellar cortex. *Ann N Y Acad Sci* **978**, 405–412.

Huang, Z.J., Di Cristo, G. & Ango, F. (2007) Development of GABA innervation in the cerebral and cerebellar cortices. *Nat Rev Neurosci* **8**, 673–686.

Iwakura, A., Uchigashima, M., Miyazaki, T., Yamasaki, M. & Watanabe, M. (2012) Lack of molecular-anatomical evidence for GABAergic influence on axon initial segment of cerebellar Purkinje cells by the pinceau formation. *J Neurosci* **32**, 9438–9448.

Kalscheuer, V.M., Tao, J., Donnelly, A., Hollway, G., Schwinger, E., Kübart, S., Menzel, C., Hoeltzenbein, M., Tommerup, N., Eyre, H., Harbord, M., Haan, E., Sutherland, G.R., Ropers, H.H. & Gécz, J. (2003) Disruption of the serine/threonine kinase 9 gene causes severe X-linked infantile spasms and mental retardation. *Am J Hum Genet* **72**, 1401–1411.

Kameshita, I., Sekiguchi, M., Hamasaki, D., Sugiyama, Y., Hatano, N., Suetake, I., Tajima, S. & Sueyoshi, N. (2008) Cyclin-dependent kinase-like 5 binds and phosphorylates DNA methyltransferase 1. *Biochem Biophys Res Commun* **377**, 1162–1167.

Kaneko, T., Fujiyama, F. & Hioki, H. (2002) Immunohistochemical localization of candidates for vesicular glutamate transporters in the rat brain. *J Comp Neurol* **444**, 39–62.

Kayakabe, M., Kakizaki, T., Kaneko, R., Sasaki, A., Nakazato, Y., Shibasaki, K., Ishizaki, Y., Saito, H., Suzuki, N., Furuya, N. & Yanagawa, Y. (2014) Motor dysfunction in cerebellar Purkinje cell-specific vesicular GABA transporter knockout mice. *Front Cell Neurosci* **7**, 286.

Kilstrup-Nielsen, C., Rusconi, L., La Montanara, P., Ciceri, D., Bergo, A., Bedogni, F. & Landsberger, N. (2012) What we know and would like to know about CDKL5 and its involvement in epileptic encephalopathy. *Neural Plast* **2012**, 728267.

Kohara, K., Kitamura, A., Morishima, M. & Tsumoto, T. (2001) Activity-dependent transfer of brain-derived neurotrophic factor to postsynaptic neurons. *Science* **291**, 2419–2423.

Kuczewski, N., Porcher, C. & Gaiarsa, J.L. (2010) Activity-dependent dendritic secretion of brain-derived neurotrophic factor modulates synaptic plasticity. *Eur J Neurosci* **32**, 1239–1244.

Lindholm, D., Castrén, E., Berzaghi, M., Blöchl, A. & Thoenen, H. (1994) Activity-dependent and hormonal regulation of neurotrophin mRNA levels in the brain – implications for neuronal plasticity. *J Neurobiol* **25**, 1362–1372.

Lindholm, D., Hamnér, S. & Zirrgiebel, U. (1997) Neurotrophins and cerebellar development. *Perspect Dev Neurobiol* **5**, 83–94.

Lonetti, G., Angelucci, A., Morando, L., Boggio, E.M., Giustetto, M. & Pizzorusso, T. (2010) Early environmental enrichment moderates the behavioral and synaptic phenotype of MeCP2 null mice. *Biol Psychiatry* **67**, 657–665.

Manent, J.B. & Represa, A. (2007) Neurotransmitters and brain maturation: early paracrine actions of GABA and glutamate modulate neuronal migration. *Neuroscientist* **13**, 268–279.

Mari, F., Azimonti, S., Bertani, I., Bolognese, F., Colombo, E., Caselli, R., Scala, E., Longo, I., Grosso, S., Pescucci, C., Ariani, F., Hayek, G., Balestri, P., Bergo, A., Badaracco, G., Zappella, M., Broccoli, V., Renieri, A., Kilstrup-Nielsen, C. & Landsberger, N. (2005) CDKL5 belongs to the same molecular pathway of MeCP2 and it is responsible for the early-onset seizure variant of Rett syndrome. *Hum Mol Genet* **14**, 1935–1946.

Massella, A., Gusciglio, M., D'Intino, G., Sivilia, S., Ferraro, L., Calzà, L. & Giardino, L. (2009) Gabapentin treatment improves motor coordination in a mice model of progressive ataxia. *Brain Res* **1301**, 135–142.

Meng, H., Gao, R., Dai, Q. & Qiao, X. (2007) Differential regulation of glutamate receptor-mediated BDNF mRNA expression in the cerebellum and its defects in stargazer mice. *Neuropharmacology* **53**, 81–91.

Montini, E., Andolfi, G., Caruso, A., Buchner, G., Walpole, S.M., Mariani, M., Consalez, G., Trump, D., Ballabio, A. & Franco, B. (1998) Identification and characterization of a novel serine-threonine kinase gene from the Xp22 region. *Genomics* **51**, 427–433.

Nakanishi, S. (2005) Synaptic mechanisms of the cerebellar cortical network. *Trends Neurosci* **28**, 93–100.

Obayashi, S. (2004) Possible mechanism for transfer of motor skill learning: implication of the cerebellum. *Cerebellum* **3**, 204–211.

Paxinos, G. & Franklin, K.B.J. (2001) *The Mouse Brain in Stereotaxic Coordinates*. Academic Press, San Diego, CA.

Ricciardi, S., Ungaro, F., Hambrock, M., Rademacher, N., Stefanelli, G., Brambilla, D., Sessa, A., Magagnotti, C., Bachi, A., Giarda, E., Verpelli, C., Kilstrup-Nielsen, C., Sala, C., Kalscheuer, V.M. & Broccoli, V. (2012) CDKL5 ensures excitatory synapse stability by reinforcing NGL-1-PSD95 interaction in the postsynaptic compartment and is impaired in patient iPSC-derived neurons. *Nat Cell Biol* **14**, 911–923.

Rusconi, L., Salvatoni, L., Giudici, L., Bertani, I., Kilstrup-Nielsen, C., Broccoli, V. & Landsberger, N. (2008) CDKL5 expression is modulated during neuronal development and its subcellular distribution is tightly regulated by the C-terminal tail. *J Biol Chem* **283**, 30101–30111.

Sekiguchi, M., Katayama, S., Hatano, N., Shigeri, Y., Sueyoshi, N. & Kameshit, I. (2013) Identification of amphiphysin 1 as an endogenous substrate for CDKL5, a protein kinase associated with X-linked neurodevelopmental disorder. *Arch Biochem Biophys* **535**, 257–267.

Stalpers, X.L., Spruijt, L., Yntema, H.G. & Verrips, A. (2012) Clinical phenotype of 5 females with a CDKL5 mutation. *J Child Neurol* **27**, 90–93.

Stroobants, S., Gantois, I., Pooters, T. & D'Hooge, R. (2013) Increased gait variability in mice with small cerebellar cortex lesions and normal rotarod performance. *Behav Brain Res* **241**, 32–37.

Suárez, J., Bermúdez-Silva, F.J., Mackie, K., Ledent, C., Zimmer, A., Cravatt, B.F. & de Fonseca, F.R. (2008) Immunohistochemical description of the endogenous cannabinoid system in the rat cerebellum and functionally related nuclei. *J Comp Neurol* **509**, 400–421.

Takayama, C. (2005) Formation of GABAergic synapses in the cerebellum. *Cerebellum* **4**, 171–177.

Tao, J., Van Esch, H., Hagedorn-Greiwe, M., Hoffmann, K., Moser, B., Raynaud, M., Sperner, J., Fryns, J.P., Schwinger, E., Gécz, J., Ropers, H.H. & Kalscheuer, V.M. (2004) Mutations in the X-linked cyclin-dependent kinase-like 5 (CDKL5/STK9) gene are associated with severe neurodevelopmental retardation. *Am J Hum Genet* **75**, 1149–1154.

Timmann, D., Citron, R., Watts, S. & Hore, J. (2001) Increased variability in finger position occurs throughout overarm throws made by cerebellar and unskilled subjects. *J Neurophysiol* **86**, 2690–2702.

Wang, I.T., Allen, M., Goffin, D., Zhu, X., Fairless, A.H., Brodkin, E.S., Siegel, S.J., Marsh, E.D., Blendy, J.A. & Zhou, Z. (2012) Loss of CDKL5 disrupts kinome profile and event-related potentials leading to autistic-like phenotypes in mice. *Proc Natl Acad Sci U S A* **109**, 21516–21521.

Weaving, L.S., Christodoulou, J., Williamson, S.L., Friend, K.L., McKenzie, O.L., Archer, H., Evans, J., Clarke, A., Pelka, G.J., Tam, P.P., Watson, C., Lahooti, H., Ellaway, C.J., Bennetts, B., Leonard, H. & Gécz, J. (2004) Mutations of CDKL5 cause a severe neurodevelopmental disorder with infantile spasms and mental retardation. *Am J Hum Genet* **75**, 1079–1093.

Wulff, P., Schonewille, M., Renzi, M., Viltono, L., Sassoè-Pognetto, M., Badura, A., Gao, Z., Hoebeek, F.E., van Dorp, S., Wisden, W., Farrant, M. & De Zeeuw, C.I. (2009) Synaptic inhibition of Purkinje cells mediates consolidation of vestibulo-cerebellar motor learning. *Nat Neurosci* **12**, 1042–1049.

Zhang, L., Chung, S.K. & Chow, B.K. (2014) The knockout of secretin in cerebellar Purkinje cells impairs mouse motor coordination and motor learning. *Neuropsychopharmacology* **39**, 1460–1468.

Acknowledgment

This work has been supported by Telethon, GGP11147 (L.C.).